Supp Fig 1

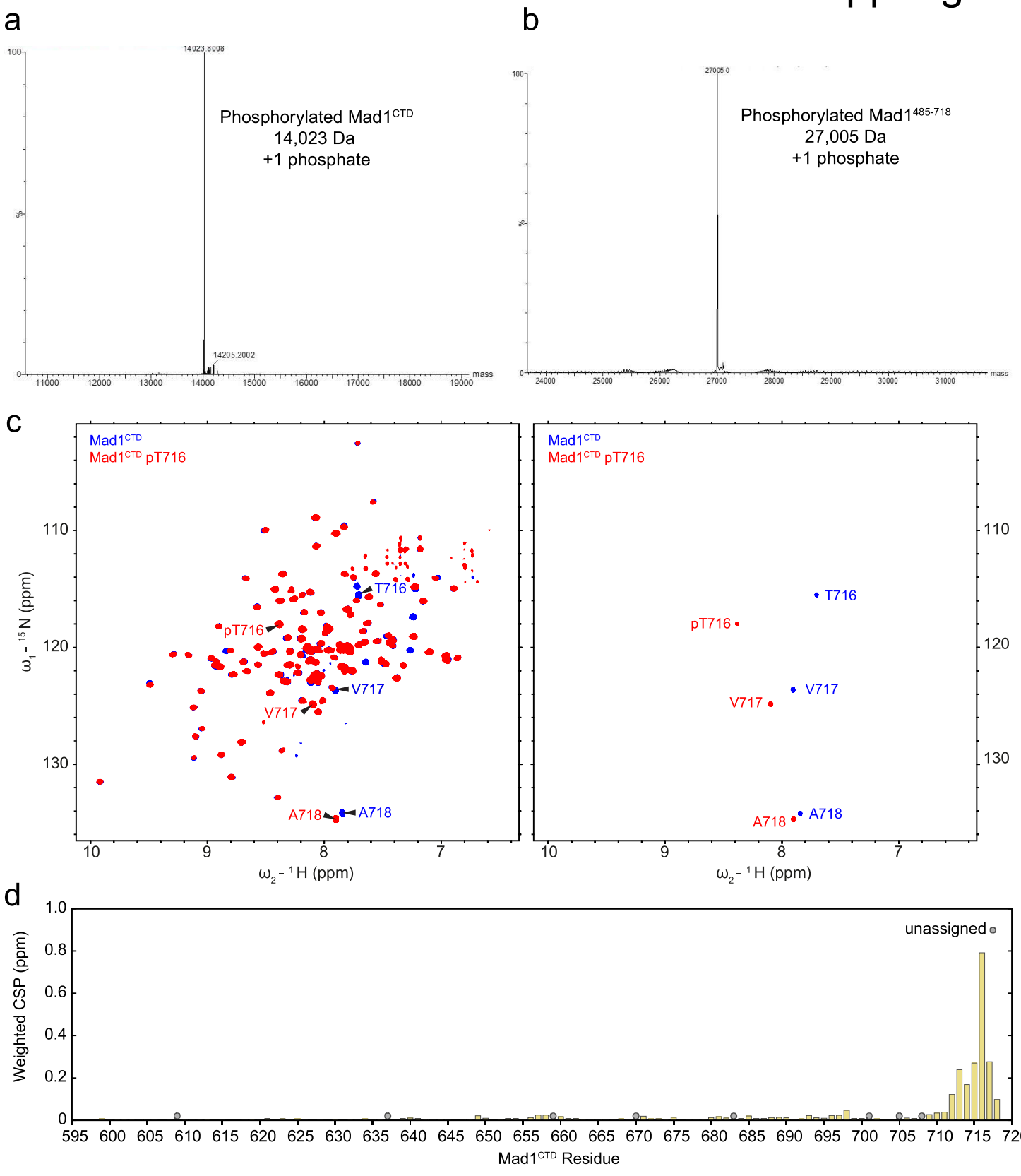
a
Phosphorylated Mad1CTD
14,023 Da
+1 phosphate
14205.2002
mass
b
Phosphorylated Mad1485-718
27,005 Da
+1 phosphate
27005.0
mass
c
Mad1CTD
Mad1CTD pT716
T716
pT716
V717
A718
ω1 - 15N (ppm)
ω2 - 1H (ppm)
d
unassigned
Weighted CSP (ppm)
Mad1CTD Residue

Supp Fig 1: Characterization of pMad1^{CTD} by intact mass spectrometry and NMR. a Mad1^{CTD} (residues 597-718) was phosphorylated by GST-Mps1 and then analysed by intact mass spectrometry. The apparent mass of the pMad1^{CTD} monomer is 14,023 Da, which is 80 Da larger than that of Mad1^{CTD} (13,943 Da), suggesting that only one residue of monomeric Mad1^{CTD} was phosphorylated by Mps1 under these conditions *in vitro.* **b** The Mad1$^{485-718}$:C-Mad2 complex was phosphorylated by GST-Mps1 *in vitro* and then analysed by intact mass spectrometry. The apparent mass of the pMad1$^{485-718}$ monomer is 27,005 Da, 80 Da larger than that of Mad1$^{485-718}$ (26,925 Da), suggesting that like Mad1^{CTD}, only one residue of monomeric Mad1$^{485-718}$ was phosphorylated by Mps1 under these conditions *in vitro.* **c** ^{1}H,^{15}N 2D HSQC showing ^{15}N-labelled Mad1^{CTD} (blue) and pMad1^{CTD} pT716 (red), shown with low (left) and high (right) contour levels. Arrows indicate the three C-terminal residues, including the phosphorylation site Thr716, identified using backbone resonances reported in our previous study[21]. As they are located in the highly flexible C-terminus, their corresponding peaks have high signal-to-noise ratios (right) and can be used to determine the extent of pThr716 phosphorylation. **d** Chemical shift perturbations observed in (c) were mapped onto the sequence of Mad1^{CTD}. Unassigned peaks are denoted as grey circles.

Supp Fig 2

a

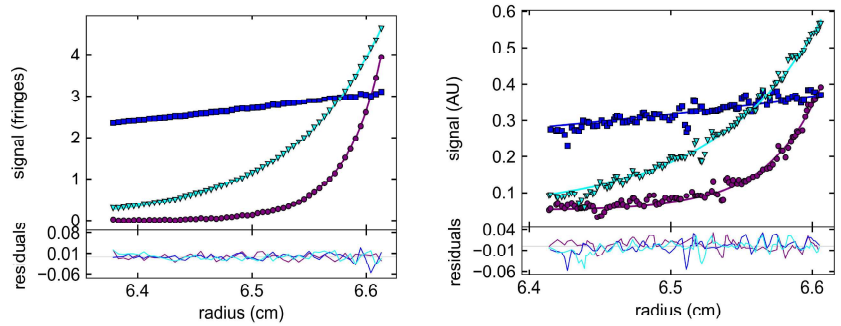

20 μM Mad1^{CTD}
Mass = 26,341 Da

b

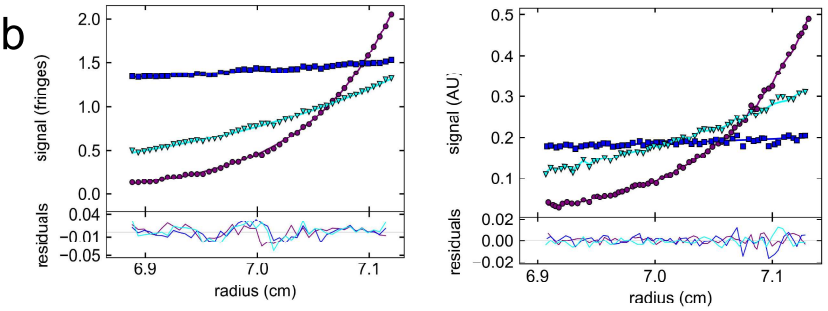

100 μM Cdc20^{N}
Mass = 7,780 Da

c

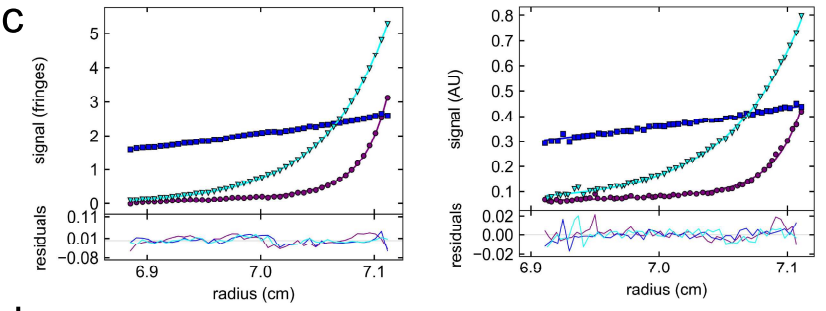

20 μM Mad1^{CTD}
40 μM Cdc20^{N}
Masses = 32,554 Da
and 7,786 Da*

d

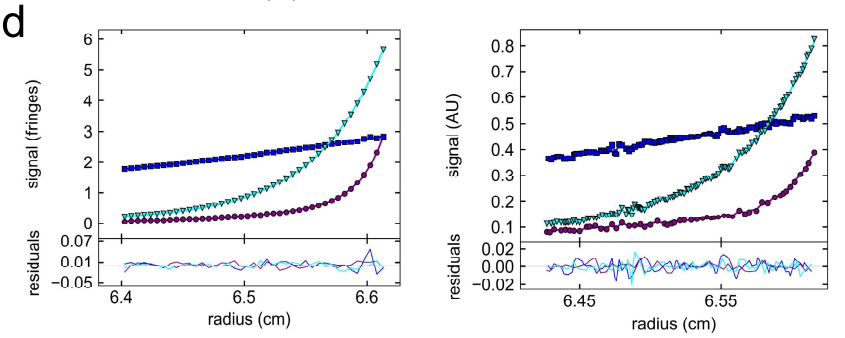

20 μM Mad1^{CTD}
80 μM Cdc20^{N}
Masses = 35,936 Da
and 7,876 Da*

Supp Fig 2: Sedimentation equilibrium (AUC-SE) of pMad1^{CTD} and Cdc20^{N}. The interference data and absorbance data are shown on the left and right panels respectively. Scans were initially fitted to single species exponentials. *When there was found to be a poor fit, the number of species was increased to two or three, and the mass of a known species (Cdc20^{N}: 7876 Da) was fixed in the fit. **a** The calculated mass for 20 µM Mad1^{CTD} pT716 was 26.3 kDa, comparable to the theoretical mass of 28 kDa for Mad1^{CTD} pT716 dimer. **b** The calculated mass for 100 µM Cdc20^{N} was 7.8 kDa, in agreement to the theoretical mass of 7.8 kDa. **c,d** The calculated mass for the major species in 20 µM Mad1^{CTD} + 40 µM Cdc20^{N} was 32.6 kDa (c) and 20 µM Mad1^{CTD} + 80µM Cdc20^{N} was 35.9 kDa (d) which are close to the expected value of a single Cdc20^{N} molecule bound to the Mad1^{CTD} dimer (35.7 kDa). The average mass for the Mad1^{CTD}:Cdc20^{N} complex across all four technical replicates was 34.7 ± 0.7 µM.

Supp Fig 3

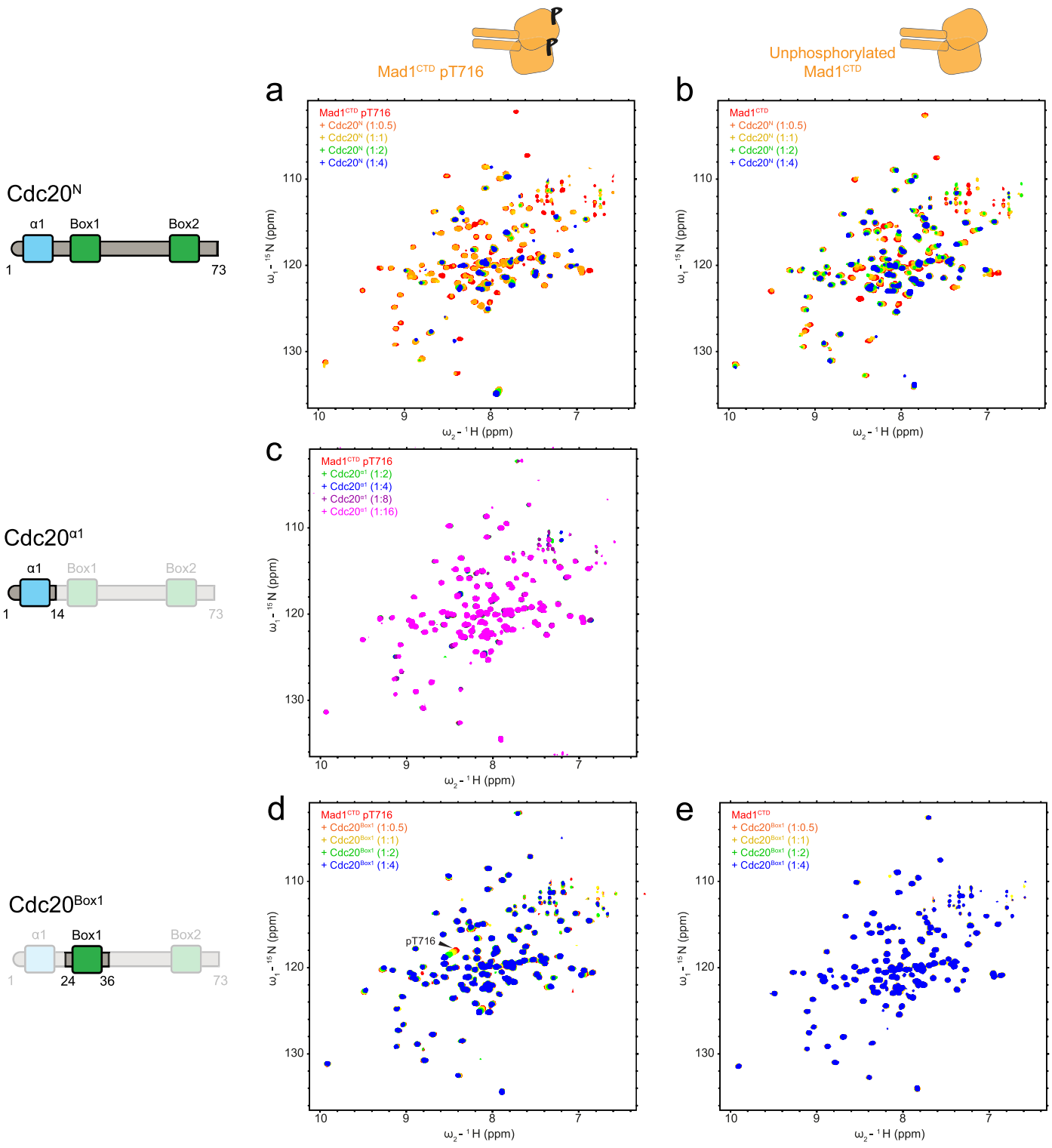
Mad1CTD pT716
Unphosphorylated Mad1CTD
Cdc20N
α1
Box1
Box2
1
73
a
Mad1CTD pT716
+ Cdc20N (1:0.5)
+ Cdc20N (1:1)
+ Cdc20N (1:2)
+ Cdc20N (1:4)
b
Mad1CTD
+ Cdc20N (1:0.5)
+ Cdc20N (1:1)
+ Cdc20N (1:2)
+ Cdc20N (1:4)
ω1 - 15N (ppm)
ω2 - 1H (ppm)
Cdc20α1
14
c
Mad1CTD pT716
+ Cdc20α1 (1:2)
+ Cdc20α1 (1:4)
+ Cdc20α1 (1:8)
+ Cdc20α1 (1:16)
Cdc20Box1
24
36
d
Mad1CTD pT716
+ Cdc20Box1 (1:0.5)
+ Cdc20Box1 (1:1)
+ Cdc20Box1 (1:2)
+ Cdc20Box1 (1:4)
pT716
e
Mad1CTD
+ Cdc20Box1 (1:0.5)
+ Cdc20Box1 (1:1)
+ Cdc20Box1 (1:2)
+ Cdc20Box1 (1:4)

Supp Fig 3: NMR spectra showing titrations of Cdc20 constructs to Mad1^{CTD}.
Cdc20 constructs were titrated into ^{15}N-labelled phosphorylated or unphosphorylated Mad1^{CTD} and analysed in ^{1}H, ^{15}N 2D HSQC. Schematics of Mad1^{CTD}, Cdc20^{N} and its specific domains indicate the analyte (top) and titrant (left) used in each experiment. **a,b** Titrating Cdc20^{N} into Mad1^{CTD} pT716 (a) or unphosphorylated Mad1^{CTD} (b). **c** Titrating Cdc20 $^{\alpha 1}$ into Mad1^{CTD} pT716. **d,e** Titrating Cdc20^{Box1} into Mad1^{CTD} pT716 (d) or unphosphorylated Mad1^{CTD} (e).

Supp Fig 4

a

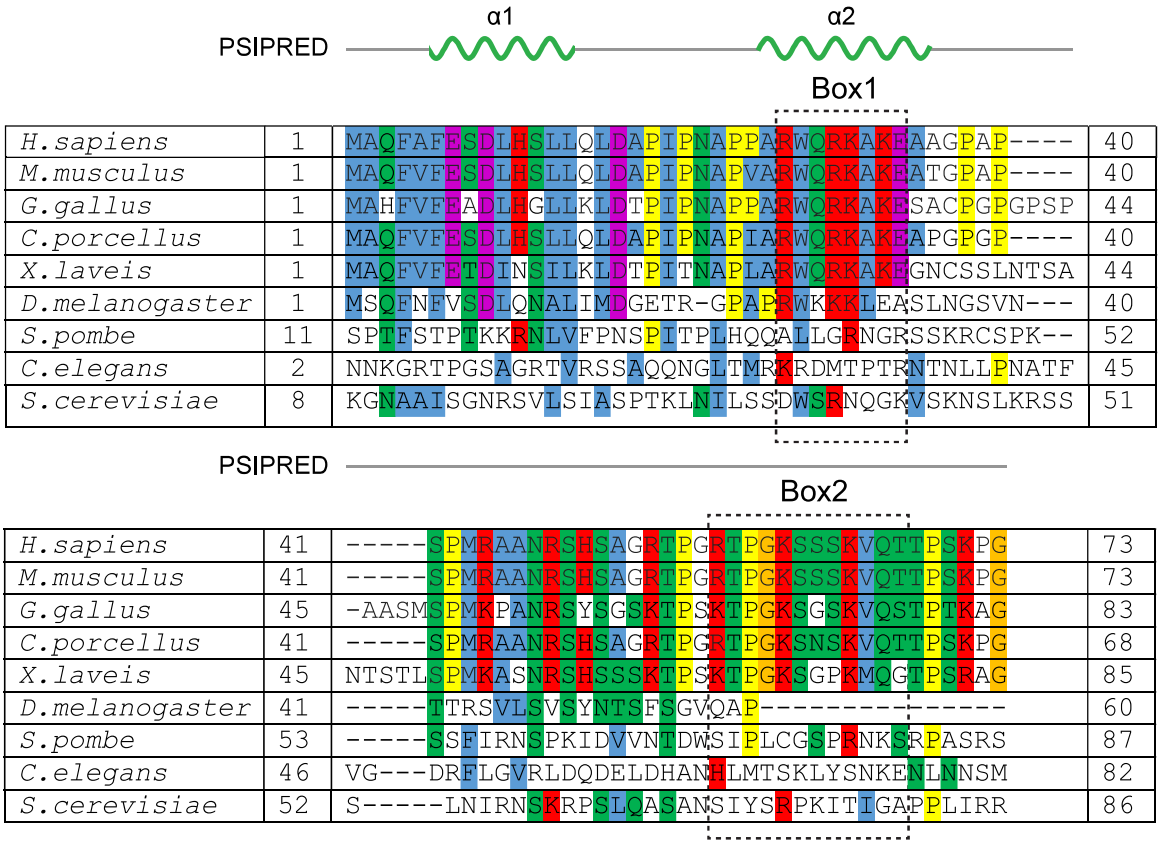
PSIPRED
α1
α2
Box1
H.sapiens 1 MAQFAFESDLHSLLQLDAPIPNAPPARWQRKAKEAAGPAP---- 40
M.musculus 1 MAQFVFESDLHSLLQLDAPIPNAPVARWQRKAKEATGPAP---- 40
G.gallus 1 MAHFVFEADLHGLLKLDTPIPNAPPARWQRKAKESACPGPGPSP 44
C.porcellus 1 MAQFVFESDLHSLLQLDAPIPNAPIARWQRKAKEAPGPGP---- 40
X.laveis 1 MAQFVFETDINSILKLDTPITNAPLARWQRKAKEGNCSSLNTSA 44
D.melanogaster 1 MSQFNFVSDLQNALIMDGETR-GPAPRWKKKLEASLNGSVN--- 40
S.pombe 11 SPTFSTPTKKRNLVFPNSPITPLHQQALLGRNGRSSKRCSPK-- 52
C.elegans 2 NNKGRTPGSAGRTVRSSAQQNGLTMRKRDMTPTRNTNLLPNATF 45
S.cerevisiae 8 KGNAAISGNRSVLSIASPTKLNILSSDWSRNQGKVSKNSLKRSS 51
PSIPRED
Box2
H.sapiens 41 -----SPMRAANRSHSAGRTPGRTPGKSSSKVQTTPSKPG 73
M.musculus 41 -----SPMRAANRSHSAGRTPGRTPGKSSSKVQTTPSKPG 73
G.gallus 45 -AASMSPMKPANRSYSGSKTPSKTPGKSGSKVQSTPTKAG 83
C.porcellus 41 -----SPMRAANRSHSAGRTPGRTPGKSNSKVQTTPSKPG 68
X.laveis 45 NTSTLSPMKASNRSHSSSKTPSKTPGKSGPKMQGTPSRAG 85
D.melanogaster 41 -----TTRSVLSVSYNTSFSGVQAP---------------- 60
S.pombe 53 -----SSFIRNSPKIDVVNTDWSIPLCGSPRNKSRPASRS 87
C.elegans 46 VG---DRFLGVRLDQDELDHANHLMTSKLYSNKENLNNSM 82
S.cerevisiae 52 S-----LNIRNSKRPSLQASANSIYSRPKITIGAPPLIRR 86

b

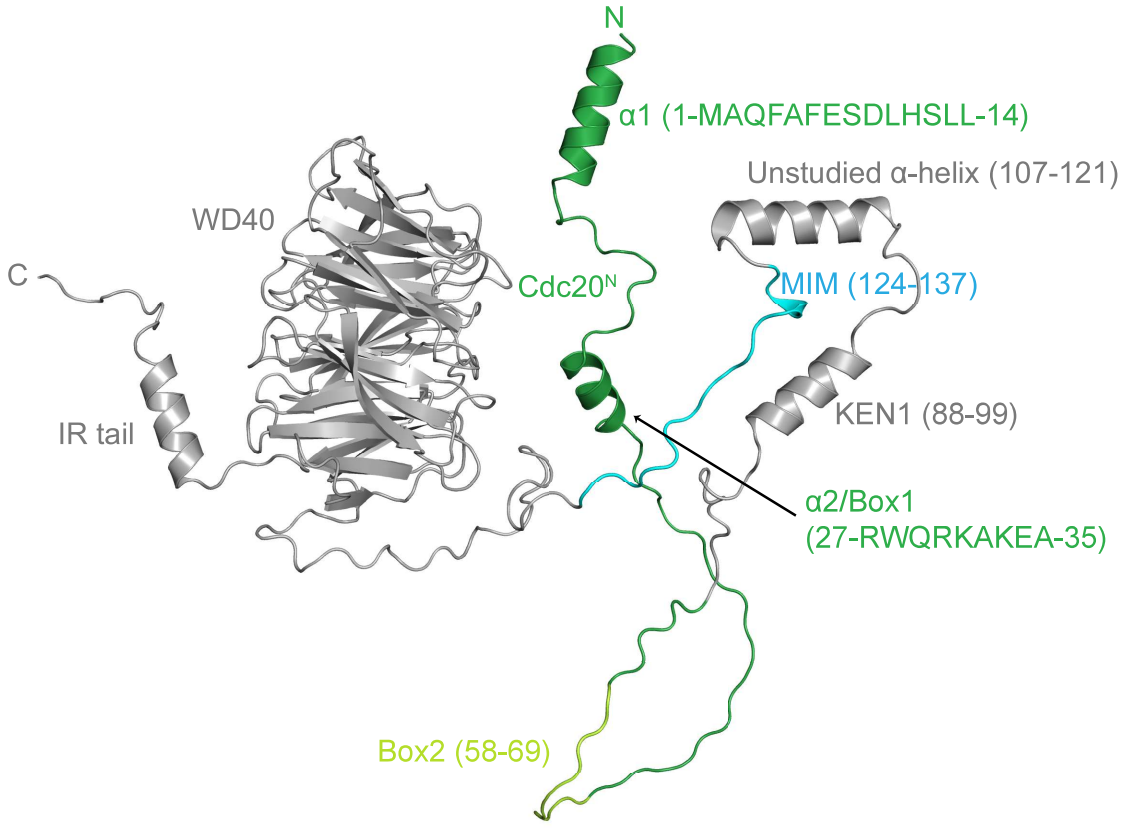
N
α1 (1-MAQFAFESDLHSLL-14)
Unstudied α-helix (107-121)
WD40
C
Cdc20N
MIM (124-137)
IR tail
KEN1 (88-99)
α2/Box1
(27-RWQRKAKEA-35)
Box2 (58-69)

Supp Fig 4: Sequence alignment and structure prediction of Cdc20. a A multiple sequence alignment of $Cdc20^{N}$. The conserved Box1 and Box2 motifs are highlighted by the dashed boxes. Secondary structure prediction by PSIPRED is shown above. **b** Structure prediction of full-length Cdc20 using AlphaFold2. $Cdc20^{N}$ is coloured in green, Box2 which has no predicted secondary structure is coloured in light green, the MIM is coloured in cyan and the rest of Cdc20 is coloured in grey.

Supp Fig 5

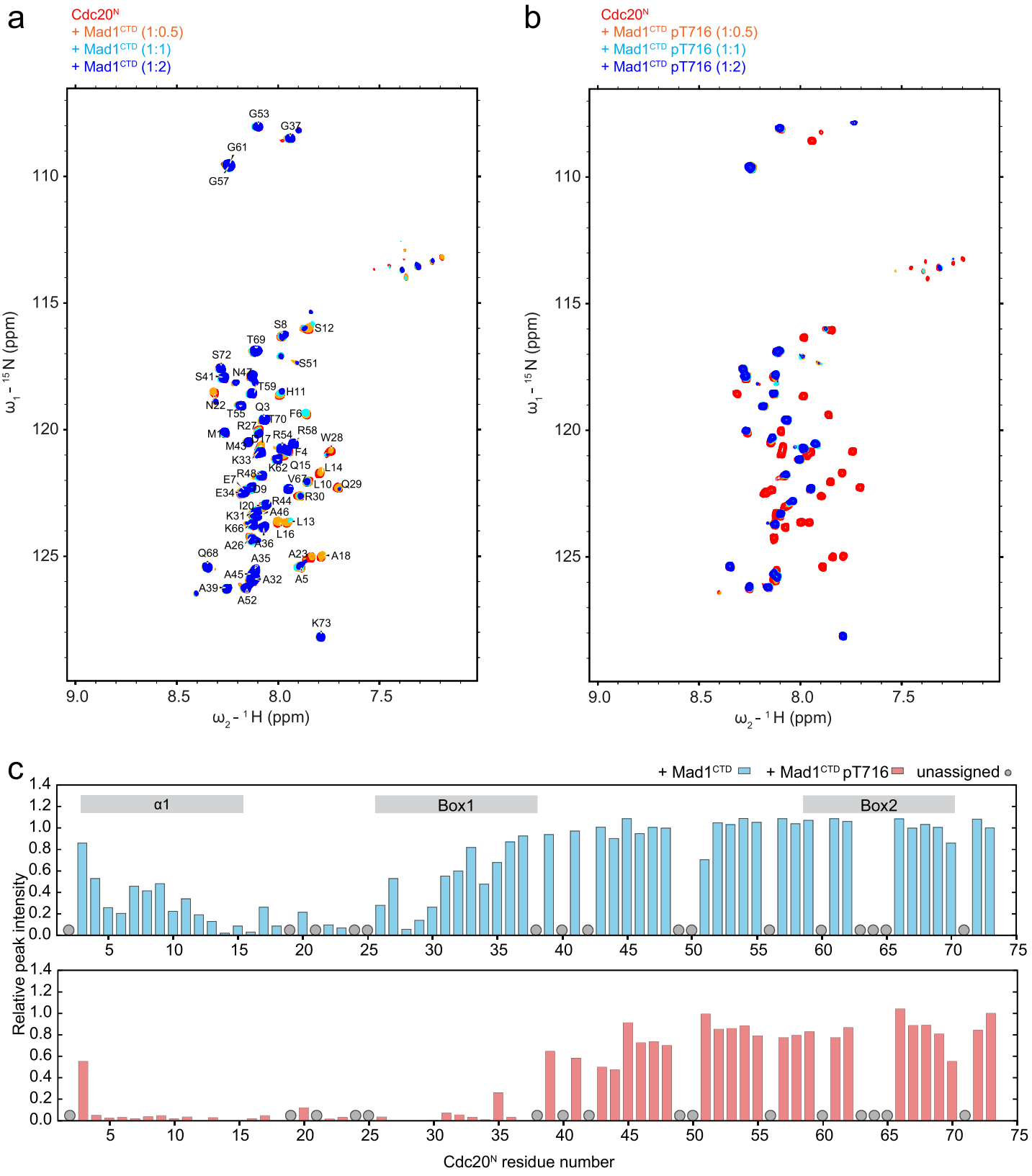
a
Cdc20N
+ Mad1CTD (1:0.5)
+ Mad1CTD (1:1)
+ Mad1CTD (1:2)
ω1 - 15N (ppm)
ω2 - 1H (ppm)
b
Cdc20N
+ Mad1CTD pT716 (1:0.5)
+ Mad1CTD pT716 (1:1)
+ Mad1CTD pT716 (1:2)
ω1 - 15N (ppm)
ω2 - 1H (ppm)
c
+ Mad1CTD
+ Mad1CTD pT716
unassigned
α1
Box1
Box2
Relative peak intensity
Cdc20N residue number

Supp Fig 5: Characterization of $Cdc20^{N}$-$Mad1^{CTD}$ interaction using ^{1}H-detected NMR. a $^{1}H,^{15}N$ 2D HSQC showing the titration of unphosphorylated $Mad1^{CTD}$ into ^{15}N-labelled $Cdc20^{N}$. Backbone resonances of $Cdc20^{N}$ are labelled with their assignment. **b** $^{1}H,^{15}N$ 2D HSQC showing the titration of $Mad1^{CTD}$ pT716 into ^{15}N-labelled $Cdc20^{N}$. **c** Relative peak intensities from the $^{1}H,^{15}N$ 2D HSQC of $Cdc20^{N}$ in the presence of phosphorylated $Mad1^{CTD}$ (blue) or $Mad1^{CTD}$pT716 (red) were mapped onto the $Cdc20^{N}$ sequence. $Mad1^{CTD}$ dimer and $Cdc20^{N}$ were mixed at 1:1 molar ratio. Peak intensities were normalized to the C-terminal residue Gly73. Multiple backbone resonances including those of prolines were absent in the $^{1}H,^{15}N$ 2D HSQC and therefore unassigned (grey circles). To achieve a more complete analysis of this interaction, ^{13}C-detected NMR were employed as shown in Fig 3a-c.

Supp Fig 6

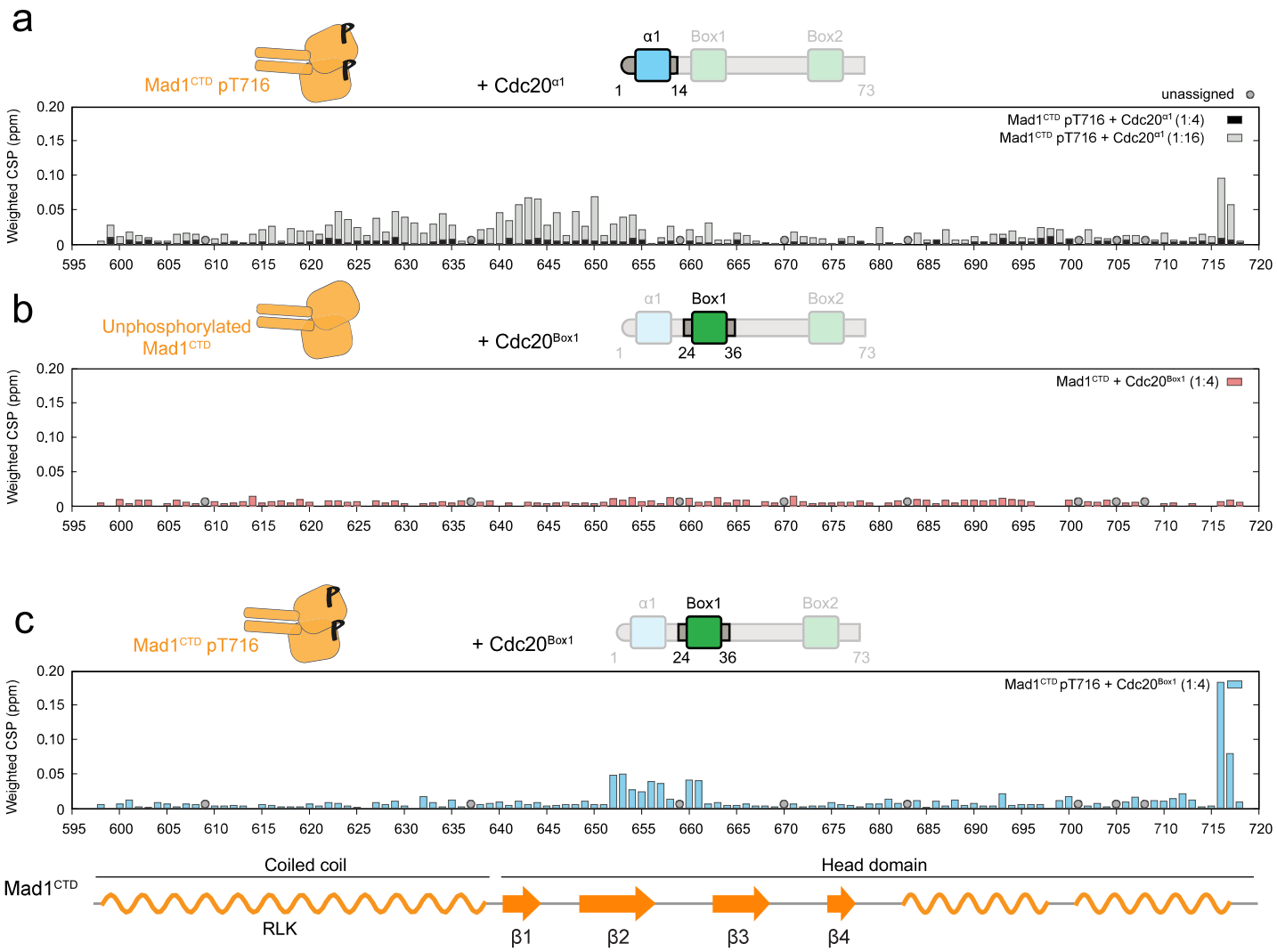
a
Mad1CTD pT716
+ Cdc20α1
α1
Box1
Box2
1
14
73
unassigned
Mad1CTD pT716 + Cdc20α1 (1:4)
Mad1CTD pT716 + Cdc20α1 (1:16)
Weighted CSP (ppm)
0.20
0.15
0.10
0.05
0
595 600 605 610 615 620 625 630 635 640 645 650 655 660 665 670 675 680 685 690 695 700 705 710 715 720
b
Unphosphorylated Mad1CTD
+ Cdc20Box1
α1
Box1
Box2
1
24
36
73
Mad1CTD + Cdc20Box1 (1:4)
Weighted CSP (ppm)
0.20
0.15
0.10
0.05
0
595 600 605 610 615 620 625 630 635 640 645 650 655 660 665 670 675 680 685 690 695 700 705 710 715 720
c
Mad1CTD pT716
+ Cdc20Box1
α1
Box1
Box2
1
24
36
73
Mad1CTD pT716 + Cdc20Box1 (1:4)
Weighted CSP (ppm)
0.20
0.15
0.10
0.05
0
595 600 605 610 615 620 625 630 635 640 645 650 655 660 665 670 675 680 685 690 695 700 705 710 715 720
Coiled coil
Head domain
Mad1CTD
RLK
β1
β2
β3
β4

Supp Fig 6: Data analysis for titrations of Cdc20$^{\alpha 1}$ and Cdc20^{Box1} peptides to ^{15}N-labelled Mad1^{CTD}. Weighted chemical shift perturbations from the ^{1}H, ^{15}N 2D HSQC of phosphorylated or unphosphorylated Mad1^{CTD} were mapped onto the Mad1^{CTD} sequence. Only chemical shift perturbations are shown because no significant change in peak intensity was observed. The schematics above each plot indicate the proteins used in each experiment. Unassigned peaks are denoted as grey circles. Secondary structure of Mad1^{CTD} is shown in the schematics below the plots. **a** Titrating Cdc20$^{\alpha 1}$ into Mad1^{CTD} pT716 from Supp Fig 3c. Spectra with two concentrations of titrants were analyzed, 1:4 in black and 1:16 in grey. It should be emphasized that these interactions are weak and CSPs were often only observable at high excess of Cdc20$^{\alpha 1}$. **b** Titrating Cdc20^{Box1} into Mad1^{CTD} pT716 from Supp Fig 3d. **c** Titrating Cdc20^{Box1} into unphosphorylated Mad1^{CTD} from Supp Fig 3e. For the Cdc20^{Box1} titrations, spectra with the highest concentration of titrants (1:4) were analysed.

Supp Fig 7

a

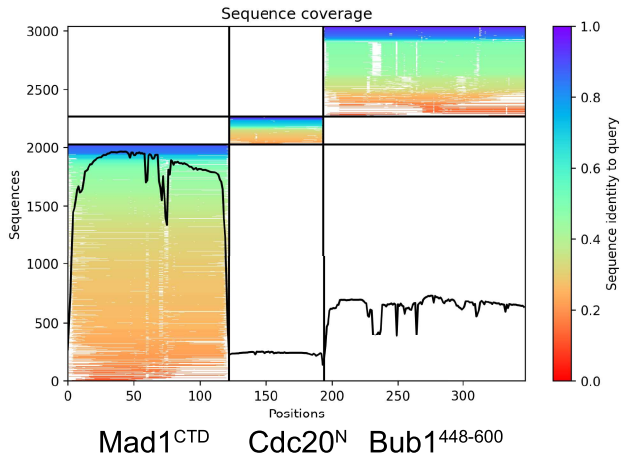

b

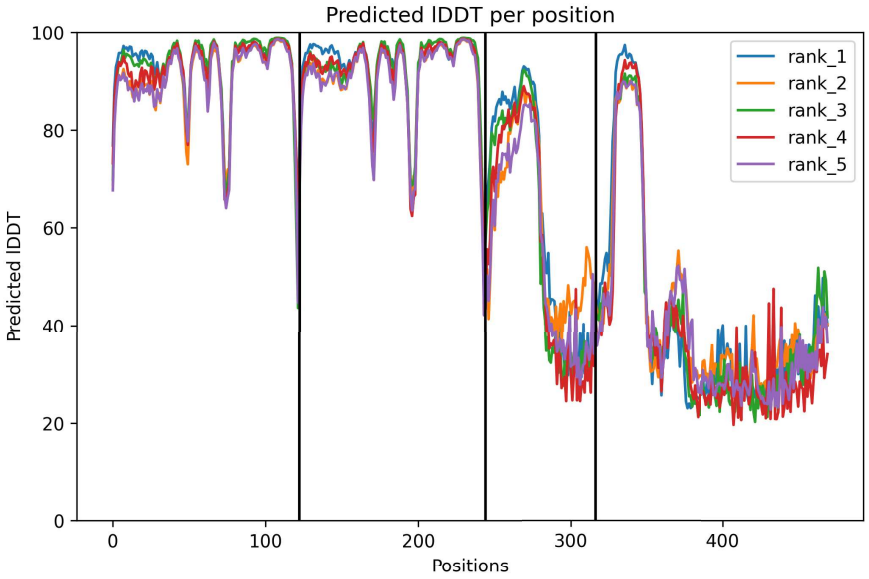

c

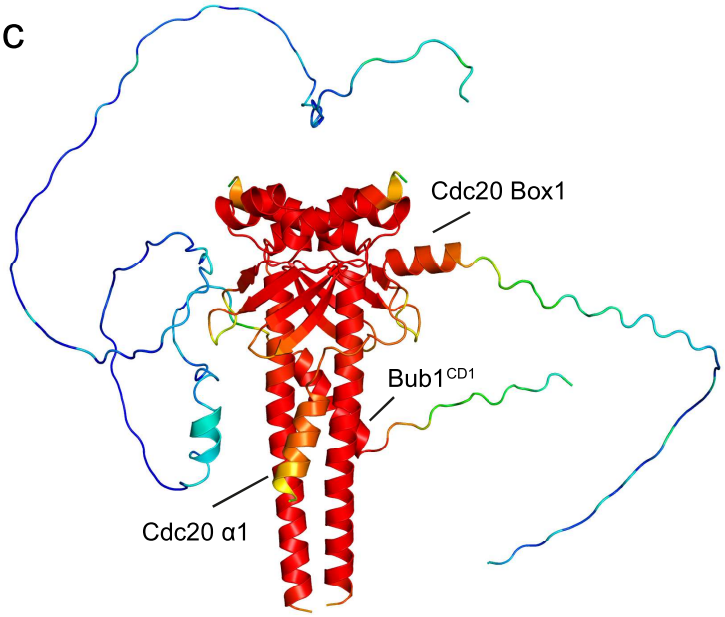

d

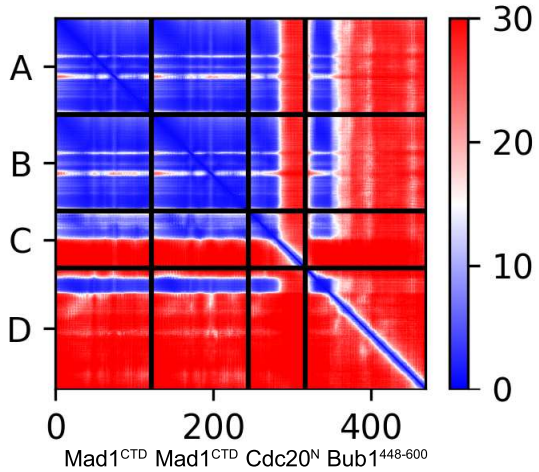

Supp Fig 7: Confidence metrics for the Bub1$^{448\text{-}600}$:Mad1^{CTD}:Cdc20^{N} AlphaFold2 prediction. a Coverage plot for the AlphaFold2 prediction multisequence alignment. Position 1-122, 123-196 and 197-350 correspond to residues 597-718 in Mad1, 1-73 in Cdc20 and 448-600 in Bub1, respectively. **b** Predicted local distance difference test (pLDDT) values for the AlphaFold2 model of Bub1$^{448\text{-}600}$:Mad1^{CTD}:Cdc20^{N}. A higher score indicates higher confidence in the prediction. **c** The pLDDT values mapped onto the predicted model of Bub1$^{448\text{-}600}$:Mad1^{CTD}:Cdc20^{N}. Residues are coloured in a scale of high (red) to low (blue) pLDDT values. The Mad1^{CTD} homodimer, Bub1^{CD1}, Cdc20$^{\alpha1}$ and Cdc20^{Box1} were all predicted with high confidence (pLDDT > 80). A region following Bub1^{CD1} was predicted to be α-helical (cyan) but with relatively low confidence (pLDDT < 60). **d** The predicted alignment error (PAE) heat map for Bub1$^{448\text{-}600}$:Mad1^{CTD}:Cdc20^{N} AlphaFold2 prediction. The PAE heat map shows the predicted error (in angstroms) between all pairs of residues, with blue indicating lower error and red indicating higher error. The PAE plot suggests high confidence for the predicted interactions between Mad1^{CTD}:Cdc20^{N} and Mad1^{CTD}:Bub1^{CD1}.

Supp Fig 8

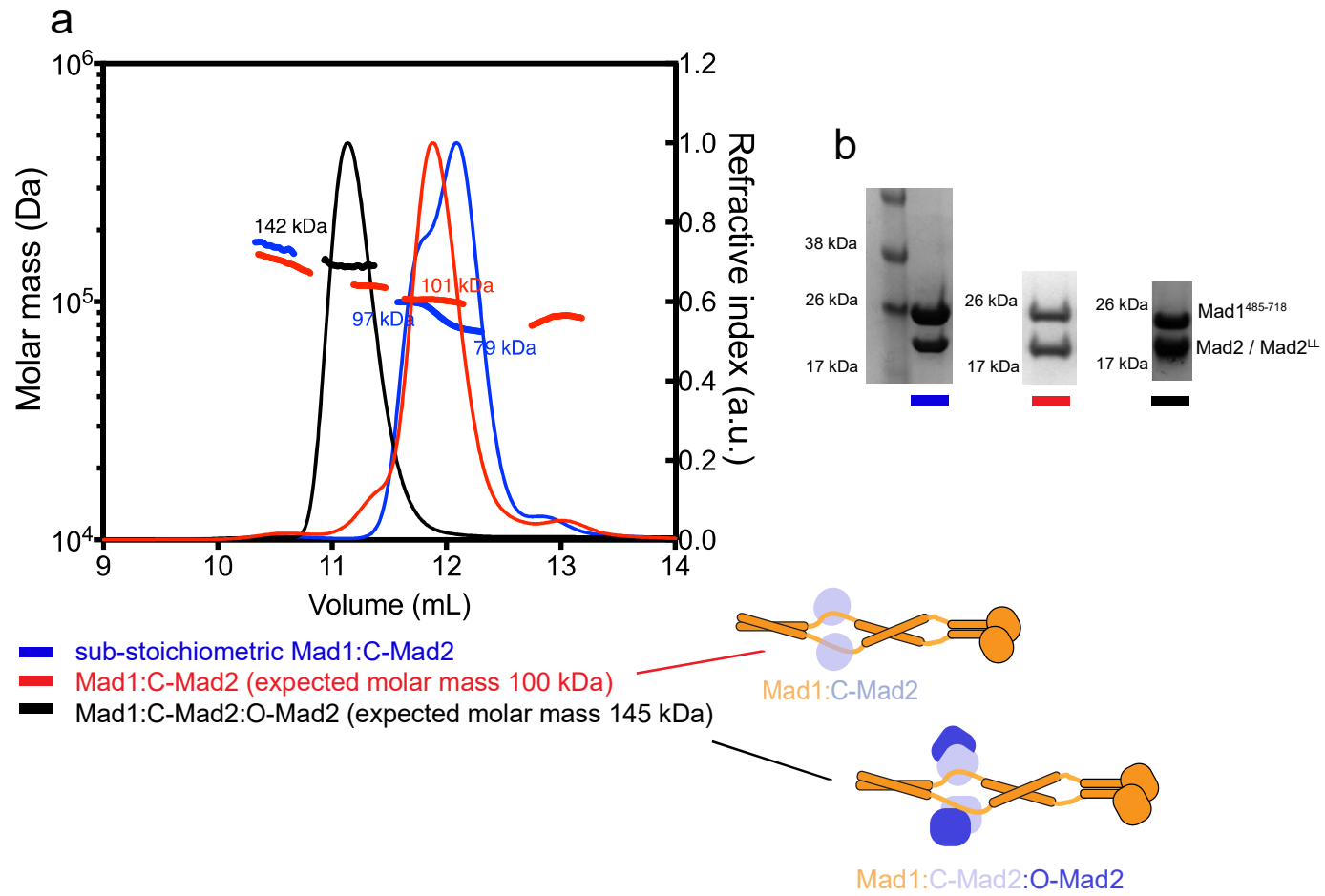
a
Molar mass (Da)
Refractive index (a.u.)
Volume (mL)
142 kDa
101 kDa
97 kDa
79 kDa
sub-stoichiometric Mad1:C-Mad2
Mad1:C-Mad2 (expected molar mass 100 kDa)
Mad1:C-Mad2:O-Mad2 (expected molar mass 145 kDa)
b
38 kDa
26 kDa
17 kDa
Mad1485-718
Mad2 / Mad2LL
Mad1:C-Mad2
Mad1:C-Mad2:O-Mad2

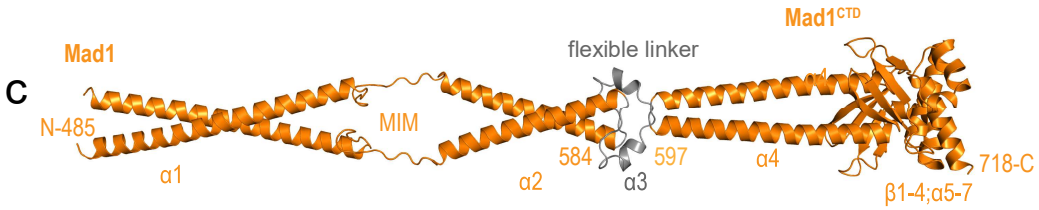
c
Mad1
N-485
α1
MIM
α2
584
α3
597
flexible linker
α4
Mad1CTD
718-C
β1-4;α5-7

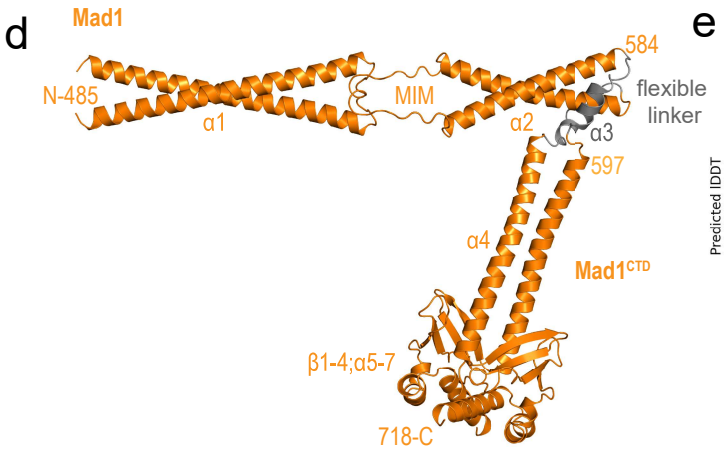
d
Mad1
N-485
α1
MIM
α2
584
α3
597
flexible linker
α4
Mad1CTD
β1-4;α5-7
718-C

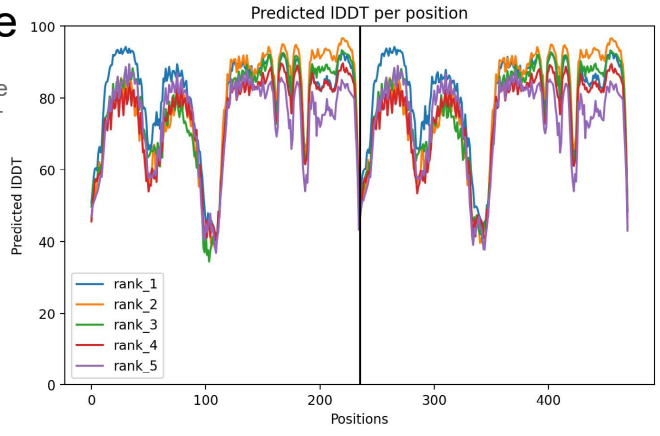
e
Predicted IDDT per position
Predicted IDDT
Positions
rank_1
rank_2
rank_3
rank_4
rank_5

Supp Fig 8: Formation of homogenous Mad1:Mad2 complexes and AlphaFold2 protein structure prediction for the Mad1 dimer. a SEC-MALS analysis of purified Mad1:Mad2 complexes, where Mad1 only contains residues 485-718. In blue is the Mad1:C-Mad2 complex purified from insect cells which is a sub-stoichiometric mixture of Mad1 dimer (expected 53 kDa), Mad1 dimer with one Mad2 molecule (expected 77 kDa), and Mad1:C-Mad2 tetramer (expected 100 kDa). In red is the homogenous Mad1:C-Mad2 tetramer after incubating the complex with excess Mad2 WT and then re-performing SEC. In black is the homogenous Mad1:C-Mad2:O-Mad2 hexamer after incubating homogenous tetramer with excess O-Mad2 (using the Mad2LL mutant described in the methods section) and re-performing SEC. Three independent measurements with similar results of each sample was completed. **b** The Mad1-Mad2 complexes outlined in (a) analysed by SDS-PAGE. **c,d** AlphaFold2 predicts the Mad1$^{485\text{-}718}$ dimer can exist in both an open-state (**c**) or a folded-state (**d**). Mad1 residues 485-584 and 597-718 are coloured orange, which includes the MIM motif. A novel short helix is predicted in the loop which disrupts the coiled-coil of α2 and α4 and is coloured grey. **e** Predicted local distance difference test (pLDDT) values for the predicted models of Mad1 dimer. A higher score indicates higher confidence in the prediction. Rank 1 model in blue is the highest ranked folded state (d) and the Rank 2 model in orange is the elongated state (c).

Supp Fig 9

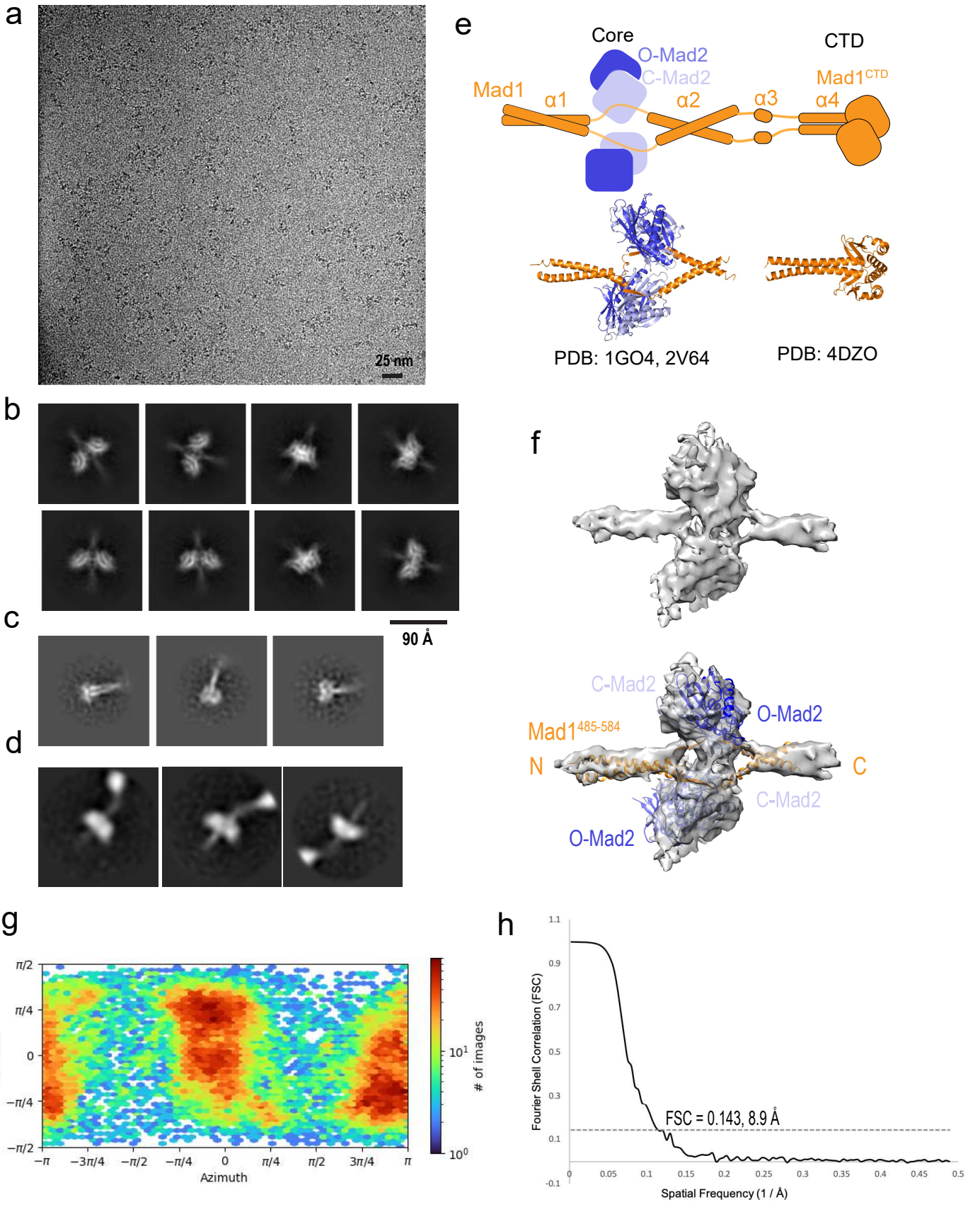
a
25 nm
b
90 Å
c
d
e
Core
O-Mad2
C-Mad2
CTD
Mad1
α1
α2
α3
α4
Mad1CTD
PDB: 1GO4, 2V64
PDB: 4DZO
f
C-Mad2
O-Mad2
Mad1485-584
N
C
C-Mad2
O-Mad2
g
Elevation
Azimuth
# of images
h
Fourier Shell Correlation (FSC)
FSC = 0.143, 8.9 Å
Spatial Frequency (1 / Å)

Supp Figure 9: Cryo-EM of unphosphorylated Mad1$^{485-718}$:C-Mad2:O-Mad2. a A representative cryo-EM micrograph from 890 total of the BS3 cross-linked Mad1:C-Mad2:O-Mad2 complex collected on a Titan Krios (ThermoFisher Scientific) 300 kV microscope equipped with a K2 detector (Gatan) in counting mode. **b** 2D averages, representative of 35 2D averages, of Mad1:C-Mad2:O-Mad2 capturing the rigid Mad2 core and the N-terminal coiled-coil and C-terminal α-helices. **c** Representative 2D averages of Mad1:C-Mad2:O-Mad2 capturing the C-terminal domain of Mad1 (Mad1^{CTD}). **d** Increasing the box size from 150 Å to 260 Å produces 2D averages which show Mad1^{CTD} flexibly tethered to the core. **e** Model diagram of Mad1:C-Mad2:O-Mad2 and the equivalent crystal structures. **f** A view of the 3D reconstruction of Mad1:C-Mad2:O-Mad2 core at 8.9Å, with the crystal structures (PDBs 1GO4 and 2V64)[23,26] fitted into the cryo-EM reconstruction below. **g** An angular distribution map calculated in cryoSPARC for particle projections. The heat map identifies the number of particles for each viewing angle. This map suggests there is a preferred orientation for the unphosphorylated Mad1:C-Mad2:O-Mad2 complex. **h** A gold-standard fourier shell correlation (FSC) of the Mad1:C-Mad2:O-Mad2 core reconstruction.

Supp Fig 10

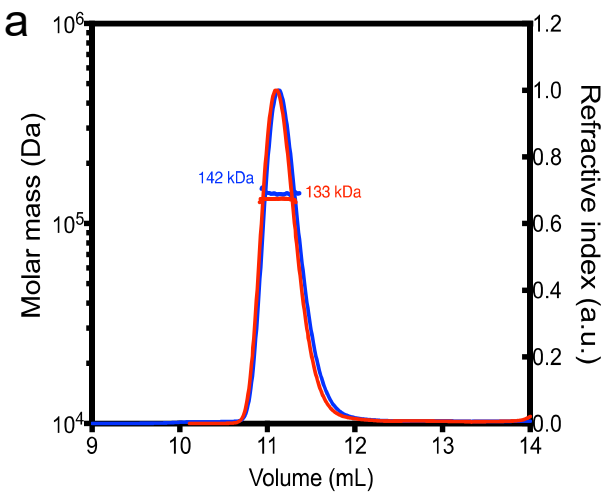
a
Molar mass (Da)
Refractive index (a.u.)
Volume (mL)
142 kDa
133 kDa

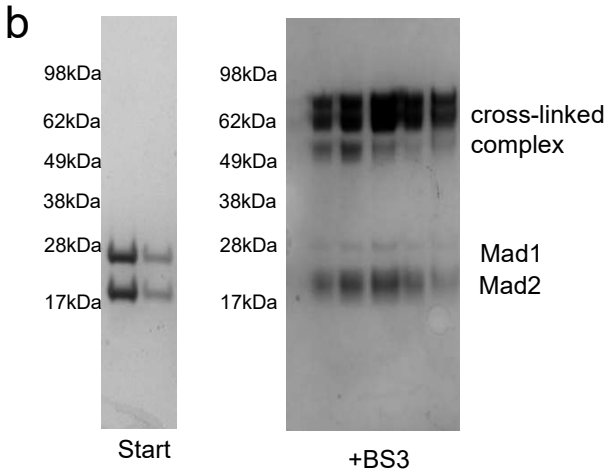
b
98kDa
62kDa
49kDa
38kDa
28kDa
17kDa
Start
+BS3
cross-linked complex
Mad1
Mad2

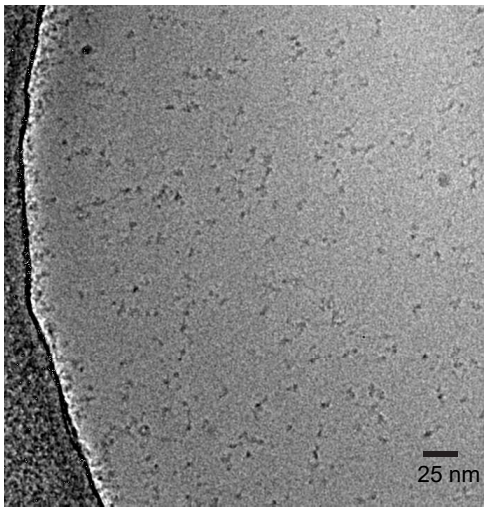
c
25 nm

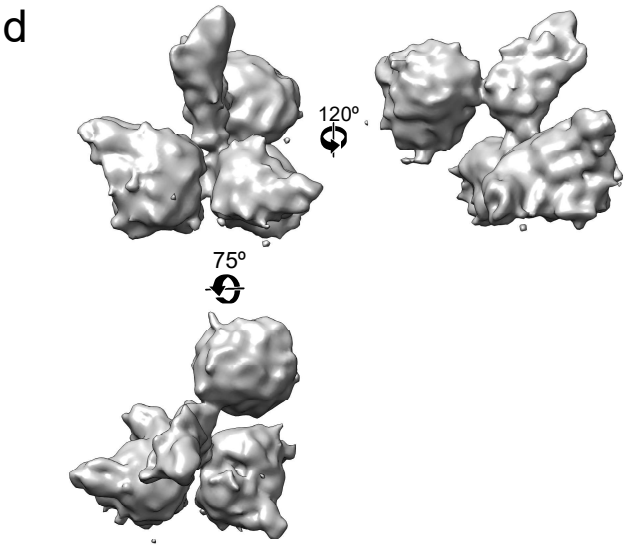
d
120°
75°

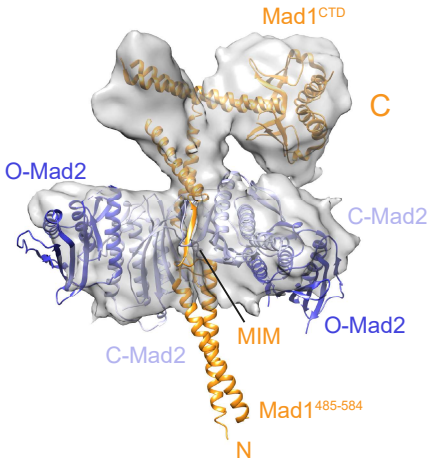
e
Mad1CTD
C
O-Mad2
C-Mad2
MIM
O-Mad2
C-Mad2
Mad1485-584
N

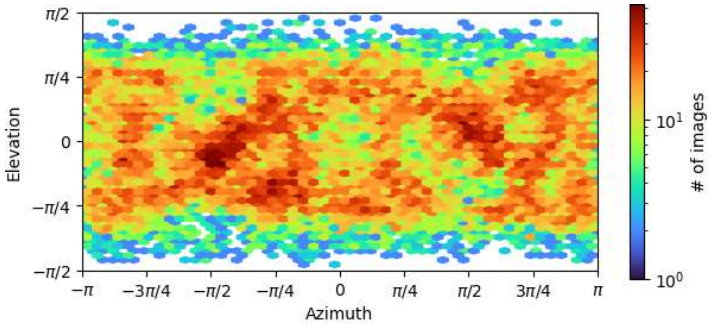
f
Elevation
Azimuth
# of images

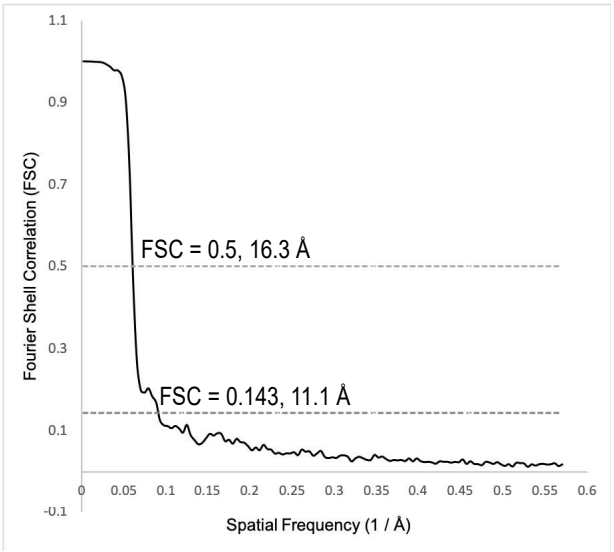
g
Fourier Shell Correlation (FSC)
FSC = 0.5, 16.3 Å
FSC = 0.143, 11.1 Å
Spatial Frequency (1 / Å)

Supp Fig 10: Supplemental cryo-EM data of phosphorylated Mad1$^{485-718}$:C-Mad2:O-Mad2. a SEC-MALS analysis of pMad1:C-Mad2:O-Mad2 before (blue) and after BS3 (red) cross-linking (expected 145 kDa). Three independent measurements were made with similar results. **b** SDS-page analysis of pMad1:C-Mad2:O-Mad2 before and after cross-linking. **c** A representative cryo-EM micrograph from 3,672 total of the pMad1:C-Mad2:O-Mad2 complex collected on a Titan Krios (ThermoFisher Scientific) 300 kV microscope equipped with a K3 detector and volta-phase plate. **d** Several views of the 3D reconstruction of the pMad1:C-Mad2:O-Mad2 complex. **e** A 3D reconstruction of pMad1:C-Mad2:O-Mad2 in a folded state with the crystal structures manually fitted into the electron density (PDBs 4DZO, 1GO4, 2V64)[23,24,26]. **f** An angular distribution map calculated in cryoSPARC for particle projections. The heat map identifies the number of particles for each viewing angle. No preferred orientation is seen, unlike the unphosphorylated Mad1:C-Mad2:O-Mad2 complex (Supp Fig 9g). **g** FSC of the pMad1:C-Mad2:O-Mad2 core reconstruction.

Supp Fig 11

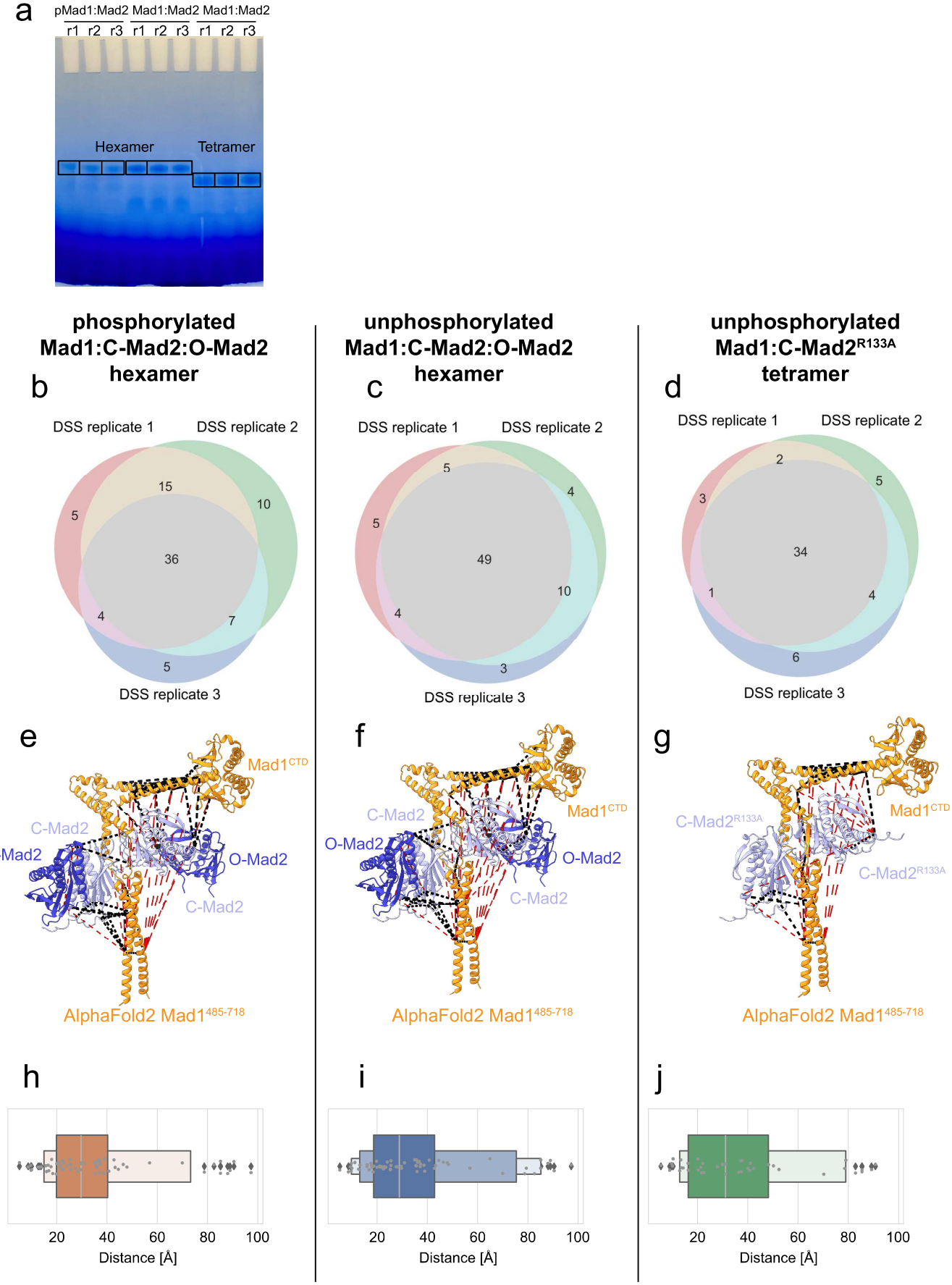
a
pMad1:Mad2 Mad1:Mad2 Mad1:Mad2
r1 r2 r3 r1 r2 r3 r1 r2 r3
Hexamer
Tetramer
phosphorylated Mad1:C-Mad2:O-Mad2 hexamer
unphosphorylated Mad1:C-Mad2:O-Mad2 hexamer
unphosphorylated Mad1:C-Mad2R133A tetramer
b
c
d
DSS replicate 1
DSS replicate 2
DSS replicate 3
15
10
5
36
4
7
5
5
4
49
10
4
3
2
5
3
34
1
4
6
e
f
g
Mad1CTD
C-Mad2
O-Mad2
O-Mad2
C-Mad2
C-Mad2
O-Mad2
Mad1CTD
O-Mad2
C-Mad2
C-Mad2R133A
Mad1CTD
C-Mad2R133A
AlphaFold2 Mad1485-718
AlphaFold2 Mad1485-718
AlphaFold2 Mad1485-718
h
i
j
20
40
60
80
100
Distance [Å]
Distance [Å]
Distance [Å]

Supp Fig 11: Overview of Mad1:Mad2 as analysed by IGX-MS. a Blue Native-PAGE of the three Mad1:Mad2 complexes analysed. Each of the boxed bands were excised, and in-gel cross-linking was performed providing three independent replicates of each sample with similar results. Homogenous Mad1:C-Mad2 tetramer formed using a dimerization deficient R133A Mad2 mutant described in the methods section was used to analyse the tetramer and ensure no super-stoichiometric amount of Mad2 was present. Venn diagrams showing the reproducibility of the IGX-MS experiments, for phosphorylated Mad1:C-Mad2:O-Mad2 (**b**), unphosphorylated Mad1:C-Mad2:O-Mad2 (**c**), and unphosphorylated Mad1:C-Mad2^{R133A} (**d**). Cross-links obtained for each sample are mapped onto the corresponding AlphaFold2 models for phosphorylated Mad1:C-Mad2:O-Mad2 (**e**), unphosphorylated Mad1:C-Mad2:O-Mad2 (**f**), and unphosphorylated Mad1:C-Mad2^{R133A} (**g**). The models were aligned onto Mad1^{MIM} using PDB 1GO4[23] for C-Mad2 and PDB 2V64[26] for O-Mad2. Mapped cross-links with a distance below 40 Å are indicated as black dashed lines and all others in red. Mad1 subunits (residues 485-718) are shown in orange, whereas closed and open Mad2 subunits (C-Mad2/O-Mad2) are coloured in light and dark blue, respectively. For all obtained cross-links, only the shortest option is depicted. **h-j** Boxen plots[81] for phosphorylated Mad1:C-Mad2:O-Mad2 (**h**), unphosphorylated Mad1:C-Mad2:O-Mad2 (**i**), and unphosphorylated Mad1:C-Mad2^{R133A} (**j**). The Boxen plots (explained in the methods section) show the obtained cross-link distances as grey dots, with outliers marked with a dark grey diamond for each sample and are used to improve visualization of the distribution of cross-link distances for Mad1:Mad2 complexes which are highly flexible and thus have more outliers. The cross-links shown are those detected in 2 out of 3 independent IGX-MS experiments. 41 total cross-links were detected in unphosphorylated Mad1:C-Mad2 tetramer, and 68 and 62 cross-links in unphosphorylated and phosphorylated Mad1:C-Mad2:O-Mad2 hexamer, respectively.

Supp Fig 12

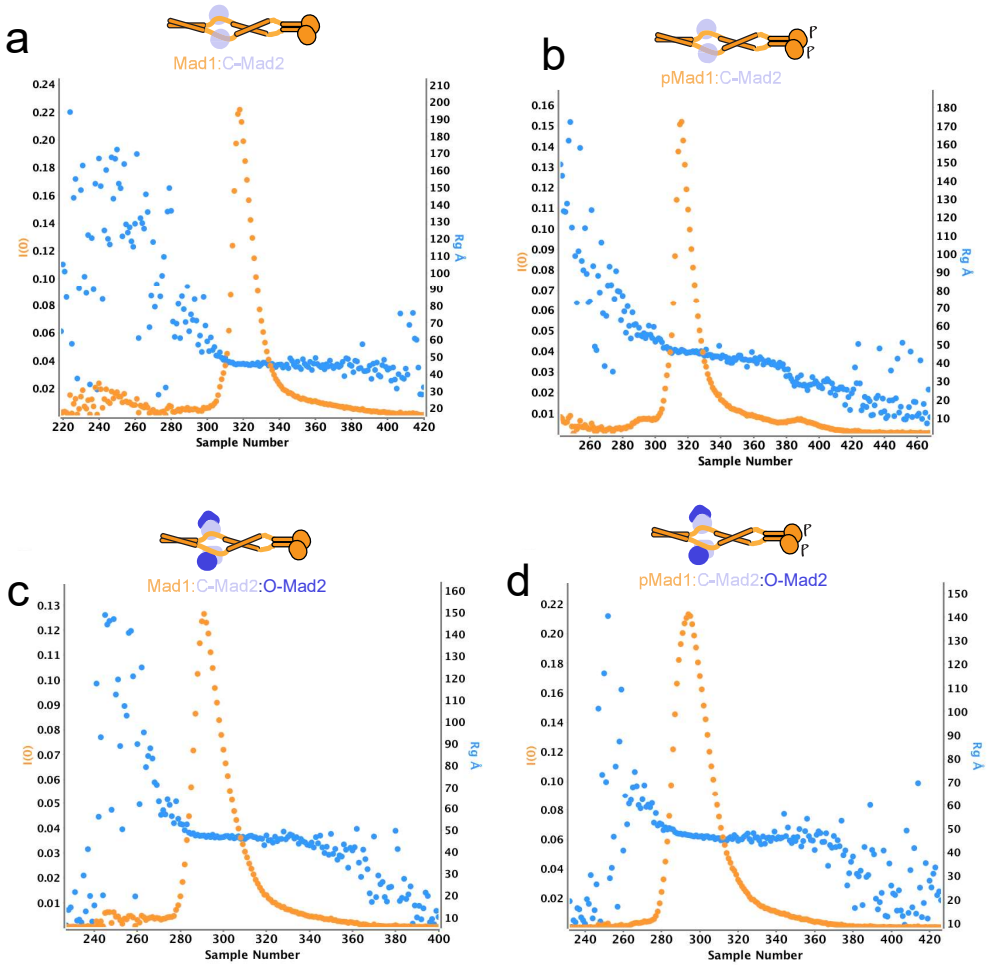
a
Mad1:C-Mad2
b
pMad1:C-Mad2
c
Mad1:C-Mad2:O-Mad2
d
pMad1:C-Mad2:O-Mad2
I(0)
Rg Å
Sample Number

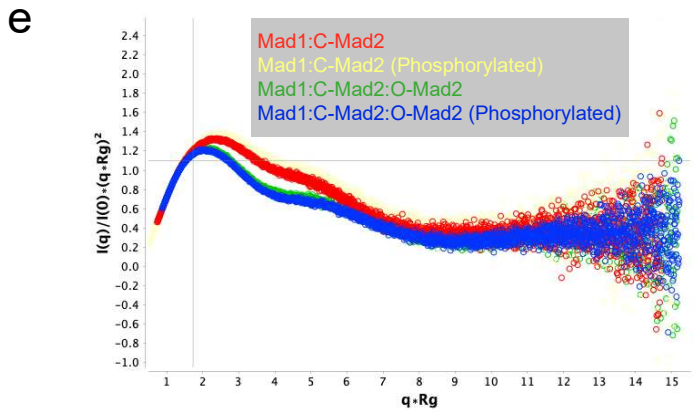
e
Mad1:C-Mad2
Mad1:C-Mad2 (Phosphorylated)
Mad1:C-Mad2:O-Mad2
Mad1:C-Mad2:O-Mad2 (Phosphorylated)
I(q)/I(0)*(q*Rg)²
q*Rg

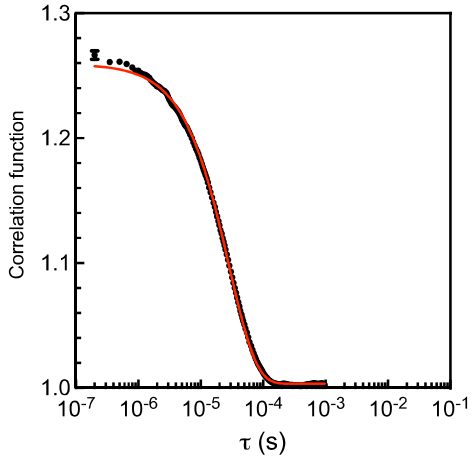
g
Correlation function
τ (s)

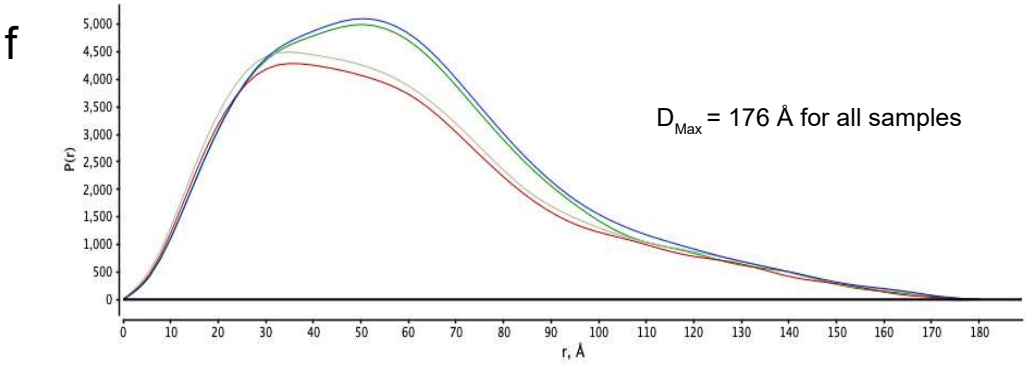
f
P(r)
r, Å
D_Max = 176 Å for all samples

Supp Fig 12: SEC-SAXS and QELS analysis of Mad1:Mad2 complexes. a-d The SEC profile with I(0) (intensity) in orange and R_g (radius of gyration) in blue estimated from the Guinier region for each subtracted frame and monitored over the entire elution peak. All Mad1:Mad2 complexes eluted as a single peak and showed a high degree of compositional homogeneity with an average R_g across the peak of 46 Å. Unphosphorylated Mad1:C-Mad2^{R133A} (a), phosphorylated Mad1:C-Mad2^{R133A} (b), unphosphorylated Mad1:C-Mad2:O-Mad2 (c), phosphorylated Mad1:C-Mad2:O-Mad2 (d). **e** A normalized Kratky plot, showing $(q \times R_g)^2 \times I(q)\backslash I(0)$ versus $q \times R_g$ where q is the spatial frequency in 1/Å, I(q) is the scattering intensity at that spatial frequency and R_g is the radius of gyration. Kratky plots can be used as a qualitative assessment of sample flexibility and suggests that the hexameric complex containing O-Mad2 is slightly less flexible than the tetrameric complex but that there is no clear difference between the phosphorylated and unphosphorylated samples. **f** The pairwise distribution function (P(r) function), calculated from the SAXS intensity curve. All pairwise distances (r, Å) between scattering points within the molecule are plotted and extend to an approximate D_{max} of 176 Å for all Mad1:Mad2 complexes. The P(r) was normalized to volume. This suggests that there is no significant difference in conformation between the samples. A fully-extended Mad1:Mad2 structure has an estimated maximum distance of 202 Å, while the folded model has an estimated maximum distance of 151 Å. **g** SEC-MALS dynamic light scattering of pMad1:C-Mad2:O-Mad2. Typical autocorrelation function from the QELS (quasi-elastic light scattering) detector of a single timepoint in the chromatographic peak in Supp Fig 8a. The Rh was determined from the fitted translational diffusion coefficient averaged across the peak (Rh = 53 Å ± 1 = 2.4%).

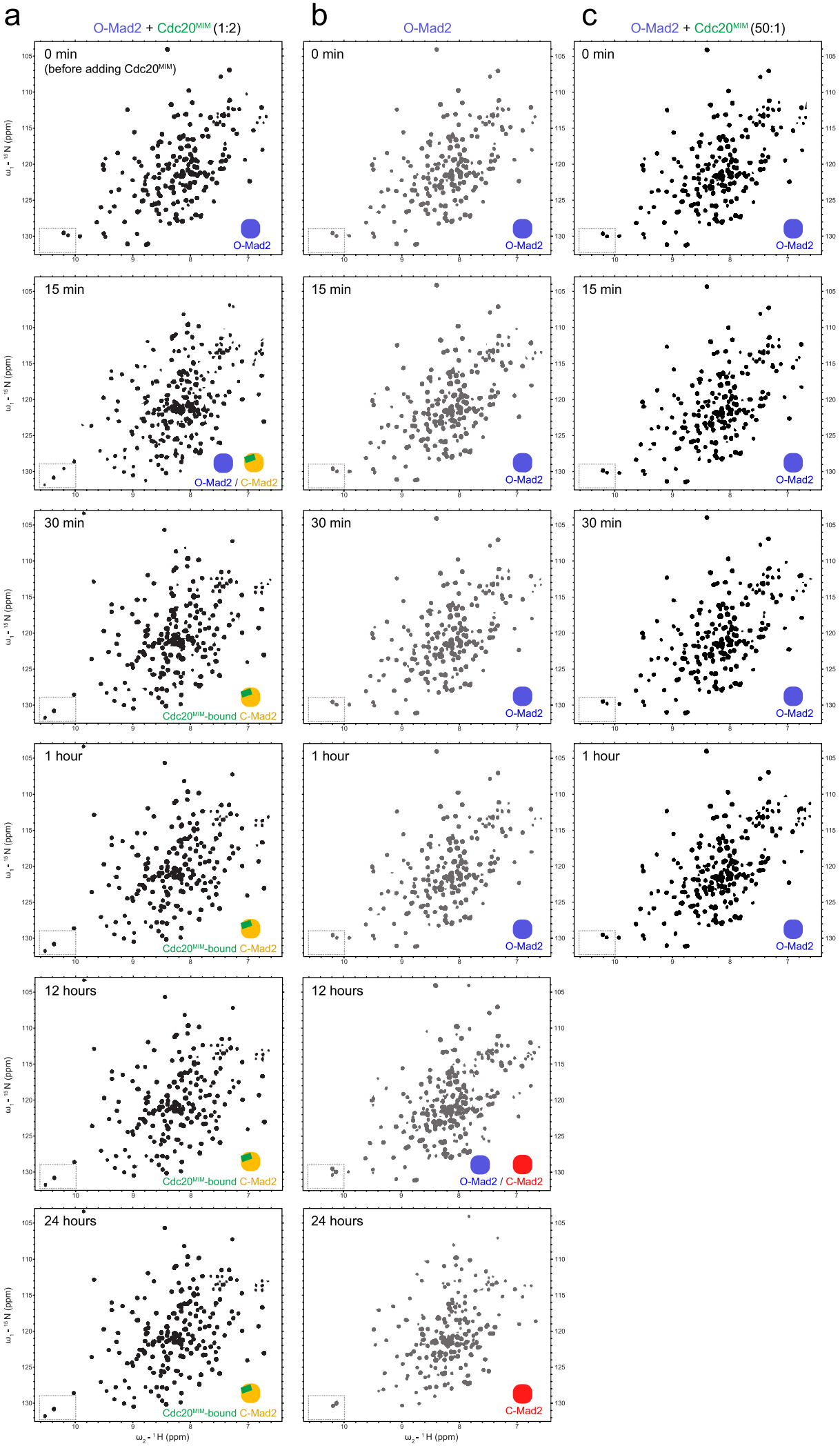
a
O-Mad2 + Cdc20MIM (1:2)
b
O-Mad2
c
O-Mad2 + Cdc20MIM (50:1)
0 min
(before adding Cdc20MIM)
15 min
30 min
1 hour
12 hours
24 hours
O-Mad2
O-Mad2 / C-Mad2
Cdc20MIM-bound C-Mad2
C-Mad2
ω1 - 15N (ppm)
ω2 - 1H (ppm)

Supp Fig 13

Supp Fig 13: The MIM of Cdc20 induces Mad2 conversion. ^{1}H, ^{15}N 2D HSQC of ^{15}N-labelled O-Mad2 during open-to-closed conversion of Mad2. **a,b** Conversion of 100 µM ^{15}N-labelled O-Mad2 R133A in the presence (a) or absence (b) of 200 µM $Cdc20^{MIM}$ peptide at 25°C. As shown in Figure 7a, the side chains of Trp167 and Trp75 are diagnostic of Mad2 conformation, and their resonances are boxed in the spectra. The schematics show the conformation of Mad2 as indicated by the tryptophan side chain resonances. **c** Substoichiometric concentration of $Cdc20^{MIM}$ was used in (c) where 2 µM of $Cdc20^{MIM}$ was added to 100 µM ^{15}N-labelled O-Mad2 R133A. The majority of Mad2 remains in an open state, in marked contrast to the spontaneous conversion observed when $Cdc20^{MIM}$ was added in a 2-fold excess (a). This suggests that $Cdc20^{MIM}$ cannot be reused in the reaction and is therefore not a catalyst for Mad2 conversion. Instead $Cdc20^{MIM}$ functions to induce conversion and stabilizes $Cdc20^{MIM}$-bound C-Mad2.

Supp Fig 14

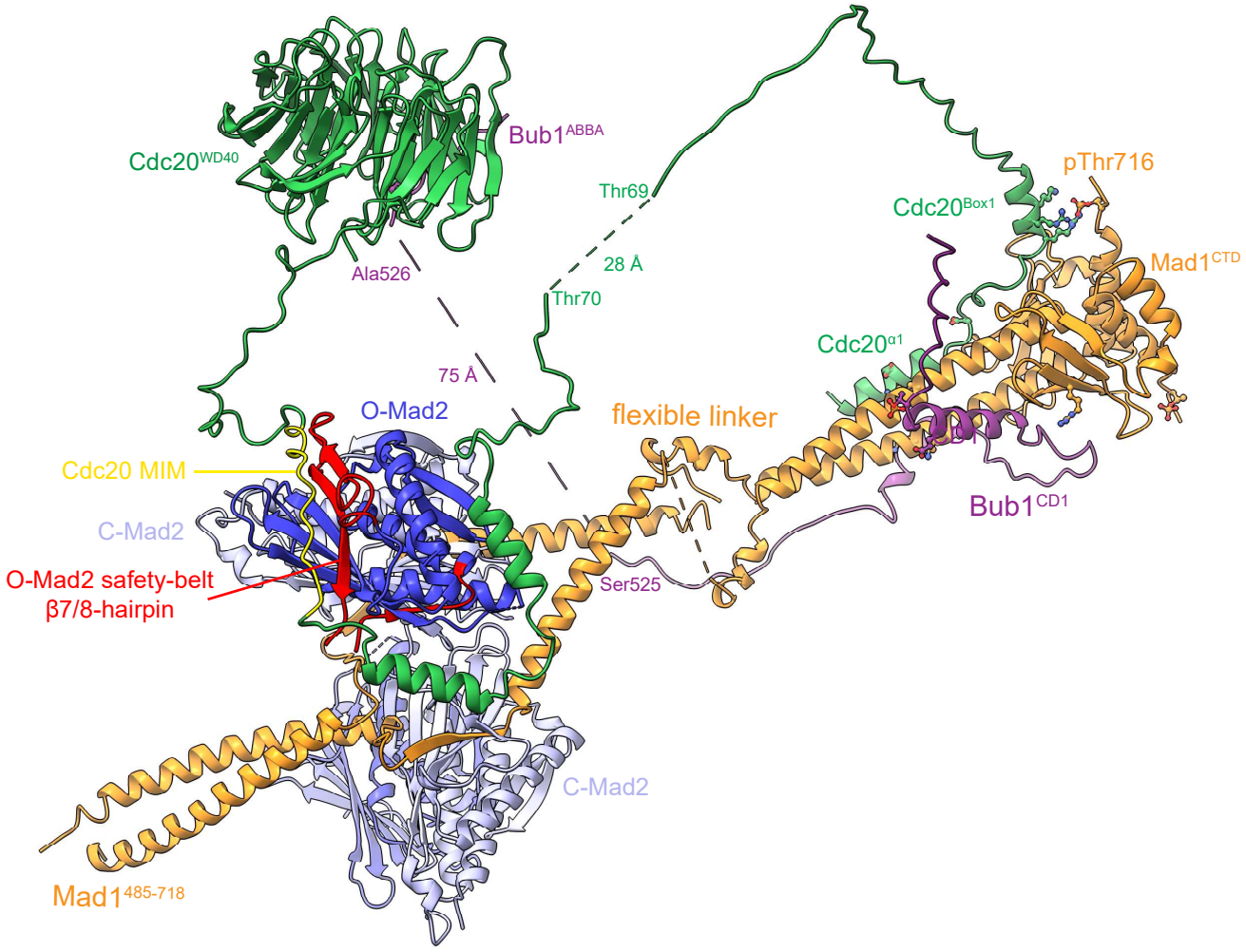
Cdc20WD40
Bub1ABBA
Ala526
Thr69
28 Å
Thr70
75 Å
pThr716
Cdc20Box1
Mad1CTD
Cdc20α1
flexible linker
O-Mad2
Cdc20 MIM
C-Mad2
O-Mad2 safety-belt
β7/8-hairpin
Ser525
Bub1CD1
C-Mad2
Mad1485-718

Supp Fig 14. Model of pBub1:Cdc20:pMad1:C-Mad2:O-Mad2 when Mad1 is in the elongated state. As compared to when Mad1 is in the folded state (Fig 7c). The model was generated using PDBs 1GO4, 2V64, 6TLJ, 7B1F[21,23,26,90] and the AlphaFold2 models of $Bub1^{448-534}$:$Mad1^{CTD}$:Cdc20 and the folded model of $Mad1^{485-718}$, and displayed using ChimeraX. Residues for the Mad1 pThr716 and $Cdc20^{Box1}$ Arg27/Arg30/Lys31, $Cdc20^{\alpha1}$ Asp9 and Mad1 Lys619, Mad1 Arg617 and Bub1 pThr461 interactions are depicted as sticks.

Supp Fig 15

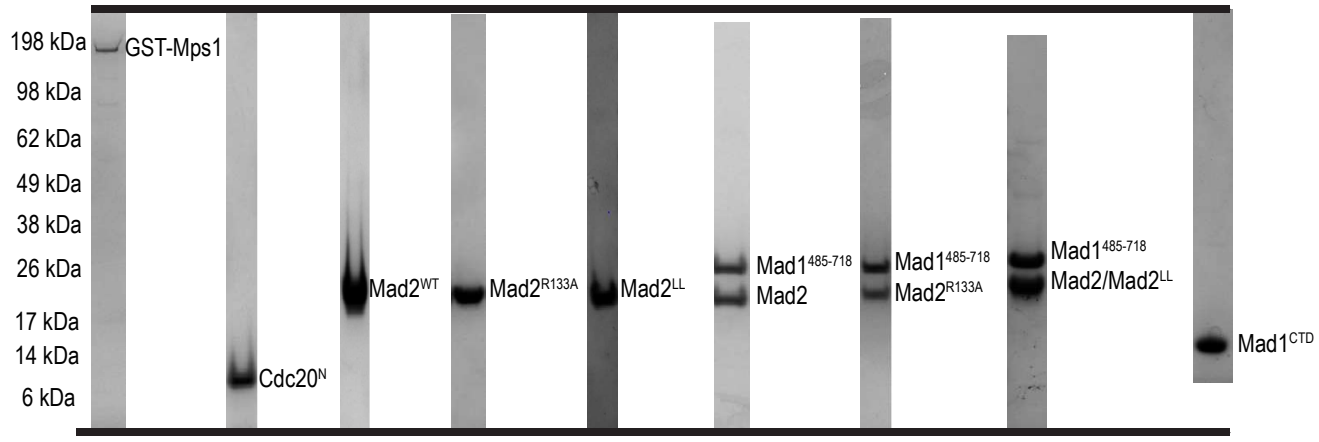
198 kDa
98 kDa
62 kDa
49 kDa
38 kDa
26 kDa
17 kDa
14 kDa
6 kDa
GST-Mps1
Cdc20N
Mad2WT
Mad2R133A
Mad2LL
Mad1485-718
Mad2
Mad1485-718
Mad2R133A
Mad1485-718
Mad2/Mad2LL
Mad1CTD

Supp Fig 15. Gallery of proteins purified in this study. All proteins were analysed by SDS-PAGE post-purification using a 4-12% Bis-Tris Glycine gel with the SeeBlue™ Plus2 Protein Ladder (ThermoFisher Scientific). Mad2LL is a mutant of Mad2 kinetically locked in the open state (O-Mad2)[26]. Mad2 R133A is a dimerization deficient mutant of Mad2 which can still bind Mad1[23].

Supp Table 1

Supp Table 1. Phosphorylation sites within Mad1^{CTD} and Mad1$^{485-718}$ when phosphorylated by full-length GST-Mps1 or the Mps1 kinase domain *in vitro*. The data obtained were compared with two prior studies (1)[ref 14] and (2)[ref 34]. For each phosphosite in this table the number of peptide spectral matches (PSMs) of the phosphorylated and corresponding unphosphorylated peptide is provided, as a semi-quantitative indication of the site occupancy. Residues which were found to be phosphorylated are shaded orange with the Thr716 site coloured in a darker shade of orange, being the only site with much more PSMs for the phosphorylated *versus* the non-phosphorylated peptide. No phosphorylated peptides were found in any of the samples prior to the *in vitro* kinase assay treatment.

Phosphorylation sites	Mad1$^{485-718}$	Mad1$^{485-718}$	Mad1^{CTD}	Mad1^{CTD}	Comparison with
Kinase	GST-Mps1	Mps1ΔKD	GST-Mps1	Mps1ΔKD	published studies
S485		1/389			1
S486		2/290			
S490		4/170			1
S494					1
T500	1/5	2/7			1
Y535					1
S538	17/121	8/46			1
T540	10/76	30/0			1
S546		2/104			1
T550	7/345	11/431			1
S551	5/11	4/17			1
S562					
S594		3/109			
S597		2/79			
S583		12/201			1
S598					1, 2
S610					2
T624					2
T644	1/200	1/212	2/300	1/103	1
T645		1/190			
S699	2/561	1/141			
S705		2/461			
T716	121/0	33/1	45/2	71/3	1, 2

Supp Table 2. Cryo-EM data-collection and 3D modelling statistics.

	Mad1$^{485-718}$:C-Mad2:O-Mad2	**pMad1$^{485-718}$:C-Mad2:O-Mad2**
Microscope	FEI Titan Krios G2	FEI Titan Krios G2
Voltage (kV)	300	300
Detector	Gatan K2	Gatan K3
Nominal magnification	105,000x	105,000x
Pixel size (Å)	1.1	0.86
Volta phase plate	No	Yes
Electron dose per frame (e^-/A^2)	1.03	1.05
Defocus range	-1.4 to -2.4	-0.5 to -1.0
Number of micrographs	890	3,672
Total number of picked particles	37,671	210,527
Number of particles used in reconstruction	13,805	33,104
Final resolution (Å)	8.9 at 0.143 FSC	11.1 at 0.143 FSC 16.3 at 0.5 FSC